

Combining ground-based with satellite-based measurements in the atmospheric state retrieval: Assessment of the information content

K. Ebell,¹ E. Orlandi,¹ A. Hünerbein,² U. Löhnert,¹ and S. Crewell¹

Received 30 November 2012; revised 21 May 2013; accepted 02 June 2013; published 3 July 2013.

[1] Remote sensing techniques offer the unique possibility to continuously and automatically monitor the atmospheric state from ground and space. Ground-based microwave radiometers (MWRs), for example, are frequently used for temperature and humidity profiling of the lower troposphere. In order to improve the profiles in the middle and upper troposphere, further information is needed. In this respect, satellite measurements are expected to be very useful. In this study, the synergy benefit in temperature and humidity clear-sky profiling using different combinations of state-of-the-art microwave and infrared ground- and satellite-based instruments is assessed. The synergy benefit is regarded as the information gain in light of ground-based MWR observations together with some climatological a priori knowledge. The maximum information content for this kind of synergy is estimated by assuming optimum conditions, e.g., no forward model uncertainties and a horizontal homogeneous atmosphere. For a midlatitude site, the ground-based MWR gives about 4.4 and 2.4 independent pieces of information on the temperature and humidity profile, respectively. For the temperature profile, the combination with Improved Atmospheric Sounding in the Infrared (IASI) and Atmospheric Microwave Sounding Unit-A/Microwave Humidity Sounder (AMSU-A/MHS) increases the information by a factor of about 1.8 and 1.5, respectively, with highest benefit in warm and/or humid conditions. The vertical information on humidity is significantly improved by highly spectrally resolved IR observations from ground or space when the atmosphere is cold and dry; the vertical information is more than tripled. If measurements from AMSU-A/MHS, IASI, or Spinning Enhanced Visible and Infrared Imager are included, retrieval uncertainties in the middle and upper troposphere are significantly reduced by up to 68%.

Citation: Ebell, K., E. Orlandi, A. Hünerbein, U. Löhnert, and S. Crewell (2013), Combining ground-based with satellite-based measurements in the atmospheric state retrieval: Assessment of the information content, *J. Geophys. Res. Atmos.*, 118, 6940–6956, doi:10.1002/jgrd.50548.

1. Introduction

[2] Accurate profiles of temperature T and humidity q are essential for climate monitoring, a better process understanding, and weather forecasting. Such profiles may not only be used to initialize and evaluate numerical weather prediction models but also to assess the atmospheric stability and to assist in nowcasting of intense convective weather. Radiosonde measurements provide this information but only typically every 12 h. Measurements of remote sensing systems which are operated on a 24/7 basis have the potential

to continuously monitor the thermodynamic state of the atmosphere. In particular, ground-based microwave (MW) radiometers (MWRs) are well-established instruments for tropospheric temperature and humidity profiling [e.g., Westwater, 1997; Güldner and Spänkuch, 2001; Crewell and Löhnert, 2007] and are operated at many sites worldwide [Hardesty et al., 2012]. Moreover, great efforts are made to set up an operational international network of MWRs in particular by the MWRnet mission (<http://cetemps.aquila.infn.it/mwrnet/>). With a harmonized data processing and quality control, the exploitation of ground-based MWR observations for the T and q profiling would be greatly facilitated.

[3] Hewison [2007] applied a variational method to retrieve profiles of temperature and total water from ground-based MWR observations. Using background information from a NWP model forecast, he showed that the number of independent pieces of information in the temperature and humidity profiles are 2.8 and 1.8, respectively. When including MWR observations at different elevation angles,

¹Institute for Geophysics and Meteorology, University of Cologne, Cologne, Germany.

²Institute for Tropospheric Research, Leipzig, Germany.

Corresponding author: K. Ebell, Institute for Geophysics and Meteorology, University of Cologne, Zùlpicher Str. 49a, DE-50674 Cologne, Germany. (kebell@meteo.uni-koeln.de)

©2013. American Geophysical Union. All Rights Reserved. 2169-897X/13/10.1002/jgrd.50548

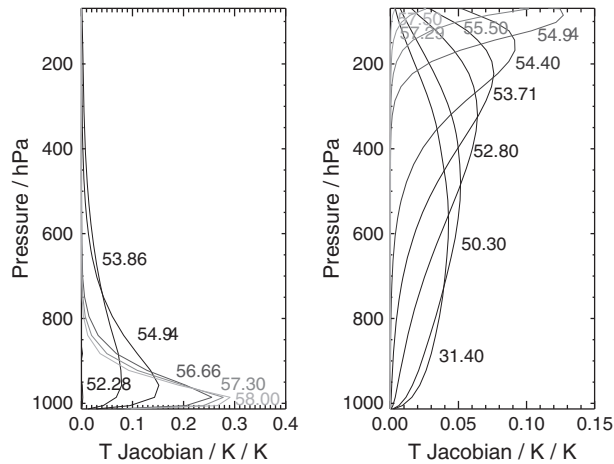


Figure 1. Temperature Jacobians for selected frequencies for a typical (left) upward and (right) downward looking MWR. For the upward looking instrument, seven frequencies (51.26–58 GHz) of the HATPRO MWR are shown, and for the downward looking instrument, the AMSU-A channels 1–9 (31.4–57.5 GHz).

the information in the temperature profile can further be increased: *Löhnert et al.* [2009], for example, found 3.5 to 4.5 (1 to 3) independent pieces of information for clear-sky temperature (humidity) MWR retrievals. They performed the analysis for a midlatitude site using a seasonal climatology as a priori information and included zenith observations as well as observations at five further elevation angles. These temperature and humidity profiles can further be improved if spectrally resolved infrared (IR) observations are included in the retrieval. The benefit of this combination is significant compared to the individual observations in cold-dry (through IR observations) and humid conditions (through MWR observations) [*Löhnert et al.*, 2009].

[4] The usage of multispectral observations in the retrieval of the atmospheric state has also been analyzed from a satellite perspective [*Eyre*, 1990; *Aires*, 2011; *Aires et al.*, 2011a, 2012]. *Aires* [2011] and *Aires et al.* [2011a, 2012] assessed the synergy of microwave (MW) and IR observations of the Atmospheric Microwave Sounding Unit-A (AMSU-A), the Microwave Humidity Sounder (MHS), and the Improved Atmospheric Sounding in the Infrared (IASI) instrument, all on board the MetOp-A satellite. In particular, *Aires et al.* [2011a] demonstrated on the basis of synthetic observations that the synergetic exploitation of the MW and IR domains is very beneficial for the retrieval of the atmospheric temperature and humidity profiles. Using a neural network inversion of both the MW and IR measurements can decrease the retrieval uncertainty by a factor of up to 2.5 (1.4) for temperature (humidity) compared to a retrieval which includes either MW or IR observations. *Aires et al.* [2012] confirmed this synergy benefit by means of real MetOp-A observations and model analysis data from the European Centre for Medium-Range Weather Forecasts (ECMWF). Furthermore, they showed that the direct combination of the different observations in the retrieval is more efficient than an a posteriori combination of the products from the single-instrument retrieval.

[5] The combination of multispectral observations is one possibility in order to enhance the accuracy of the retrieved thermodynamic profiles. Combining measurements from different viewing geometries can also increase the information of the atmospheric state. Assuming horizontal homogeneity in the direct vicinity (~ 3 km) of a ground-based MWR, *Crewell and Löhnert* [2007] have shown that best performance for temperature profiling is achieved when the MWR brightness temperatures at different frequencies and different elevation angles are included in the retrieval. By doing so, the number of independent pieces of information in the temperature profiles is on the order of 4 in contrast to 2 pieces of information using observations at zenith only [*Löhnert et al.*, 2009].

[6] However, the shortcoming of ground-based observations is that the vertical resolution of the retrieved thermodynamic profiles degrades with increasing height. For the T profile, for example, about 95% of the measurement information from a ground-based MWR is located below 4 km [*Löhnert and Maier*, 2012]. Satellite information could therefore provide complementary information as illustrated exemplarily by temperature Jacobians for selected MW frequencies mainly along the 60 GHz oxygen absorption complex for typical ground- and satellite-based MWRs (Figure 1). From a ground (satellite)-based perspective, the Jacobians for the frequencies close to the center of the absorption complex peak in very low (high) altitudes. While the maximum T sensitivity of the ground-based observations is located at heights below the 800 hPa level, the corresponding satellite observations are most sensitive to T variations above 500 hPa. Thus, it is expected that the combination of ground-based and satellite observations improves the estimates of the atmospheric state considerably compared to a retrieval using ground-based observations only. Satellite measurements alone provide valuable information for global climate monitoring, but their synergy benefit via data assimilation has also been recognized for numerical weather prediction (NWP). In particular, measurements by AMSU-A, MHS, and IASI are currently assimilated in global NWP models and provide the most valuable information in terms of forecast error reduction [*Cardinali*, 2009; *Hilton et al.*, 2012].

[7] In this paper, we analyze the synergy benefit in clear-sky tropospheric T and q profiling not only with respect to different spectral observations, i.e., in the MW and IR, but also with respect to different viewing geometries. The theoretical study is performed for synthetic observations of state-of-the-art ground- and satellite-based passive MW and IR instrumentation. Since ground-based MWRs are becoming more and more a standard and robust tool for tropospheric T and q profiling, the ground-based MWR retrieval is regarded as the baseline retrieval which the retrievals using other instrument combinations are compared to. Synergy benefit is thus here defined as the additional information and the reduction of the retrieval uncertainty compared to a retrieval using ground-based MWR observations alone.

[8] The analysis is conducted for a typical midlatitude site with the assumption that some prior knowledge of the T and q profiles, i.e., the climatological mean profiles, exists.

[9] The key questions addressed in this study can be summarized as follows: Given some climatological a priori knowledge on the atmospheric state as well as realistic

Table 1. Sensors and Channels Used in This Study

Instrument	Frequency (GHz) Wavelength (μm) Wave Number (cm^{-1})	Number of Forward Measurements	Model
<i>Ground Based</i>			
HATPRO	22.24–31.4 GHz	7	PAMTRA
	51.26–58 GHz	7	
	53.86–58 GHz	20 ^a	
AERI	538–588 cm^{-1}	104	LBLRTM
	675–713 cm^{-1}	79	
	1250–1350 cm^{-1}	207	
<i>Satellite Based</i>			
AMSU-A	23.8, 31.4, 50.3–57.617, 89 GHz	15	PAMTRA
MHS	89., 157., 184.311, 186.311, 190.311 GHz	5	PAMTRA
IASI	675–713 cm^{-1}	153	LBLRTM
	1250–1350 cm^{-1}	401	LBLRTM
SEVIRI	6.2, 7.3, 8.7, 9.7, 10.8, 12, 13.4 μm	7	RTTOV

^aMeasurements for four frequencies between 53.86 and 58 GHz at 42°, 30°, 10.2°, 19.2°, and 5.4° elevation above horizon.

a priori and measurement uncertainties, how much information on the tropospheric T and q profiles is added to ground-based MWR observations by further ground- and satellite-based sensors? Does the synergy benefit depend on the atmospheric situation? How does the a priori accuracy affect the results?

[10] First, the different ground-based and satellite sensors are described (section 2). In section 3, the experimental design of the study is presented including a detailed description of the method, models, and data being used. Section 4 encompasses the analysis of the information content of the measurements and the retrieval uncertainty. In section 5, the results are discussed, final conclusions drawn, and next steps in the ground-based/satellite-based instrument synergy presented.

2. Instruments and Channel Selection

[11] In the following, the remote sensing instruments used in this study will be presented. A list of these instruments together with the channels, typical measurement uncertainties, and forward models used to simulate the observations can be found in Table 1. From a ground-based perspective, two instruments are accounted for, the 14-channel Humidity and Temperature MWR Profiler HATPRO and the Atmospheric Emitted Radiance Interferometer AERI. Both instruments are commercially available and are operated at the Jülich Observatory for Cloud Evolution JOYCE, for example (<http://www.geomet.uni-koeln.de/en/general/research/joyce>).

[12] Corresponding MW and IR observations from satellites are provided by the AMSU-A, MHS, and IASI instruments of the polar-orbiting MetOp satellites. In addition, IR channels of the Spinning Enhanced Visible and Infrared Imager (SEVIRI) instrument are included in the analysis.

2.1. HATPRO

[13] The Humidity and Temperature Profiler (HATPRO) is a MWR measuring brightness temperatures in 14 channels. To this end, direct detection receivers within two frequency bands are utilized [Rose *et al.*, 2005]. The seven

K-band channels (22.24, 23.04, 23.84, 25.44, 26.24, 27.84, and 31.40 GHz) are in the vicinity of the 22.235 GHz water vapor absorption band, while the seven V-band channels (51.26, 52.28, 53.86, 54.94, 56.66, 57.30, and 58.00 GHz) are located within the oxygen absorption complex at 60 GHz. Brightness temperatures of the first seven channels are typically used to derive integrated water vapor and liquid water path as well as water vapor profiles. Channels in the second band are instead used to obtain temperature profiles. A steerable parabolic mirror makes HATPRO capable of performing elevation scans from -90° to $+90^\circ$ zenith angles. This feature is used to enhance the accuracy of temperature profiles in the boundary layer (cf. section 1). The antenna half power beam width (HPBW) for the water vapor channels is 3.5° , while the temperature sounding channels' antenna has a HPBW of 2.5° . Typical random instrument noise values are 0.1 K for the K-band and 0.2 K for the V-Band channels [Radiometer Physics GmbH, 2011].

2.2. AERI

[14] The Atmospheric Emitted Radiance Interferometer (AERI) is a ground-based passive IR interferometer. Downwelling radiances are measured from 520 to 3020 cm^{-1} (corresponding to wavelengths between 19 and 3 μm) at 1 cm^{-1} resolution. A detailed description on the instrument design and performance can be found in Knuteson *et al.* [2004a, 2004b]. For the average noise level in clear-sky cases [Knuteson *et al.*, 2004b], typical random instrument noise is estimated to be 0.01 $\text{mW m}^{-2} \text{sr}^{-1} \text{cm}$ at high wave numbers to 1.8 $\text{mW m}^{-2} \text{sr}^{-1} \text{cm}$ at low wave numbers [Löhnert *et al.*, 2009].

[15] A typical measurement cycle of AERI consists of a 3 min averaging of sky radiance spectra and the subsequent observation of the two black body targets. The whole measurement process lasts about 8 min. Since the AERI performs the self-calibration after each sky view, any temperature drifts in the black body or the internal temperature are accounted for. The field of view of the AERI is 2.6° (46 mrad) HPBW.

[16] The AERI spectra contain information on the vertical temperature and water vapor profiles [Feltz *et al.*, 1998; Smith *et al.*, 1999; Feltz *et al.*, 2003]. Measurements from the CO_2 bands at 15 and 4.3 μm , i.e., 612–713 cm^{-1} and 2223–2260 cm^{-1} , have been used to retrieve temperature profiles, while spectral observations from the wings of the $\sim 18 \mu\text{m}$ rotational and 6.3 μm water vapor bands, corresponding to 538–588 cm^{-1} and 1250–1350 cm^{-1} , have been utilized for humidity profiling. Löhnert *et al.* [2009] analyzed the information content of AERI and HATPRO measurements in temperature and humidity profiles using almost the same spectral bands. They excluded the 612–660 cm^{-1} observations of the 15 μm CO_2 band which provide no additional information compared to the 675–713 cm^{-1} observations and are associated with higher noise values. In the present study, we focus on three AERI bands, namely, 538–588 cm^{-1} , 675–713 cm^{-1} , and 1250–1350 cm^{-1} , but exclude the band on the shortwave side (2223–2260 cm^{-1}) where scattering of sunlight by atmospheric gases during daytime can complicate the retrieval application. Note that we only account for thermal emission and absorption in the radiative transfer model which is used to simulate the AERI observations.

2.3. AMSU-A and MHS

[17] The Advanced Microwave Sounding Unit-A AMSU-A and the Microwave Humidity Sounder MHS are radiometers measuring brightness temperatures at different viewing angles as they scan the Earth perpendicularly to the satellite direction of motion. AMSU-A has 12 channels around the 50–60 GHz oxygen absorption complex and three window channels at 23.8, 31.4, and 89 GHz [NOAA, 2009]. The AMSU-A radiometer was designed to provide information on temperature from about 3 hPa (45 km) to the surface. The MHS instrument has three channels around the 183.311 GHz absorption line and two window channels at 89 and 157 GHz. MHS measurements are used to derive profiles of water vapor in the troposphere [Klaes *et al.*, 2007]. Typical values for the uncertainties of the AMSU-A and MHS channels range between 0.22 K and 1.2 K [NOAA, 2009]. The routine assimilation of brightness temperatures from both instruments in NWP models significantly improves the forecast error [Cardinali, 2009].

[18] AMSU-A uses a stepwise scan concept, with its scanning mirror stopped at a fixed position during the integration time. It measures brightness temperatures at 30 different scanning angles, from -48.3° to $+48.3^\circ$ nadir angle [NOAA, 2009] corresponding to an Earth incidence angle of 57.3° . The swath width is ~ 2000 km. AMSU-A's HPBW is 3.38° , resulting in spot size of $48 \text{ km} \times 48 \text{ km}$ at nadir, degrading to $147 \text{ km} \times 79 \text{ km}$ at the edges of the swath. A two-point calibration of AMSU-A is performed at every scan by rotating the mirror to look at the cold space and at an internal calibration target whose temperature is monitored with multiple precision thermistors.

[19] The MHS instrument has the same swath width as AMSU-A but a horizontal resolution three times higher (1.11°), resulting in 90 equidistant angular positions for each scan line. MHS's horizontal resolution is $16 \text{ km} \times 16 \text{ km}$ at nadir, degrading to $53 \text{ km} \times 27 \text{ km}$ at the edges of the swath. The scan time of MHS and AMSU-A instruments has been arranged in such a way that three subsequent MHS scans (comprehensive of three calibrations) take the same time (8 s) as one scan of AMSU-A, resulting in a coherent scan pattern with ~ 9 MHS spots enclosed within one AMSU-A spot.

[20] AMSU-A and MHS instruments are always deployed in tandem on Low Earth Orbit (LEO) satellites [Klaes *et al.*, 2007]. At present, the AMSU-A/MHS suite is flown on eight LEO satellite platforms: EUMETSAT polar system satellites MetOp-A and MetOp-B, NOAA-15 to NOAA-19 satellites, and the Aqua platform. Note that NOAA-15 to NOAA-17 satellites deploy a heritage version of the MHS instrument, AMSU-B. The Aqua satellite uses instead the Humidity Sounder for Brazil, HSB. Both instruments have characteristics similar to MHS.

2.4. SEVIRI

[21] The SEVIRI [Schmetz *et al.*, 2002] instruments are on board the Meteosat Second Generation (MSG) geostationary satellites providing a view on Europe and Africa. SEVIRI is a radiometer which covers the visible, the near IR, and the thermal IR spectral region with 12 channels. The short-term radiometric performance of SEVIRI is reported to be between 0.1 and 0.37 K [Schmetz *et al.*, 2002]. The

high-resolution broadband visible channel provides measurements with a resolution of $1 \text{ km} \times 1 \text{ km}$, while all other channels have a resolution of $3 \text{ km} \times 3 \text{ km}$ at nadir and about $3 \text{ km} \times 6 \text{ km}$ at the midlatitudes. Earth imaging is obtained by a bidimensional Earth scan combining the satellite spin and a rotating scan mirror. The baseline measurement mode of MSG is a repeat cycle of the full Earth disc every 15 min at a position at 0° longitude. This mode allows for the monitoring of the daily cycle of weather patterns. In this study, the focus is on the thermal IR channels, i.e., 6.2, 7.3, 8.7, 9.7, 10.8, 12.0, and $13.4 \mu\text{m}$. The $6.2 \mu\text{m}$ and $7.3 \mu\text{m}$ channels are used to determine the water vapor distribution of the middle and upper troposphere. The three window channels $8.7 \mu\text{m}$, $10.8 \mu\text{m}$, and $12.0 \mu\text{m}$ can provide information on the temperature of clouds, as well as land and sea surfaces. The $9.7 \mu\text{m}$ and the $13.4 \mu\text{m}$ channels belong to the ozone and CO_2 absorption bands, respectively, and are used to provide information on the atmospheric air mass. For our study, the $3.9 \mu\text{m}$ near IR channel has the disadvantage that in the daytime the contribution due to solar radiation is not negligible. According to the AERI band selection, we thus exclude this channel in the T and q retrieval.

2.5. IASI

[22] The Infrared Atmospheric Sounding Interferometer IASI on board the MetOp-A and MetOp-B LEO satellites is a Michelson interferometer covering the IR spectral domain from 645 to 2760 cm^{-1} (corresponding to wavelengths between 3.62 and $15.5 \mu\text{m}$) [Chalon *et al.*, 2001]. IASI measures the IR radiation emitted from the Earth's atmosphere with a spectral resolution of 0.25 cm^{-1} , resulting in 8461 channels divided in three bands (645 – 1210 cm^{-1} , 1210 – 2000 cm^{-1} , and 2000 – 2760 cm^{-1}).

[23] IASI scans the Earth's surface like AMSU in a cross-tracking way with $\pm 48^\circ$ nadir angle. The resulting swath width is ~ 2000 km divided into 30 fields of view, each containing a 2×2 array of 12 km footprints. The circular 12 km footprint degrades at the swath edges to $39 \text{ km} \times 20 \text{ km}$ [EUMETSAT, 2012].

[24] The IASI interferometer was designed for high-resolution atmospheric sounding of temperature and humidity and for the retrieval of column-integrated trace gas concentrations (CO_2 , O_3 , N_2O , CO , and CH_4). Radiances measured by the IASI instrument are currently assimilated in global NWP models and show a strong positive impact on the short-range forecast capability [Cardinali, 2009; Hilton *et al.*, 2012].

[25] The calibration of the IASI interferometer is performed by looking at the cold space and at an internal black body after every 8 s swath. The noise equivalent brightness temperatures of the IASI design specification are between 0.28 K and 0.58 K [Hilton *et al.*, 2012]. In the present study, we have chosen the same spectral regions as used for the AERI instrument (see Table 1) except for the 538 – 588 cm^{-1} region which is not covered by IASI.

[26] The scanning patterns of IASI, AMSU-A and MHS, on the MetOp satellites have been coordinated in such a way that they have the same swath width and observe the same scene within 8 s [see EUMETSAT, 2012]. Note that twice a day, MetOp-A observations cover the whole globe with increasing repetition time at high latitudes. Similar instruments, the Atmospheric Infrared Sounder (AIRS) and the

Cross-track Infrared Sounder (CrIS), are currently deployed on the Aqua and Suomi National Polar-orbiting Partnership satellites, respectively. CrIs will also be part of the future Joint Polar Satellite System (JPSS) thus leading to multiple overpasses per day at a given ground-based station.

3. Experiment Setup

[27] One challenging aspect in combining different ground-based and satellite instruments is the temporal and spatial matching of the data. Due to the different field of views of the single instruments, the representativeness of a measurement for the atmospheric column to be characterized needs to be assessed. Especially when combining ground-based with satellite observations, this representativeness error can be significant and needs to be taken into account. However, in this study, we start with the simplest case and assume horizontally homogeneous, aerosol-free atmospheric conditions. Thus, we assume that all sensors see the same atmospheric scene. In particular, all polar-orbiting satellite-based sensors are assumed to be nadir-looking. The ground-based instruments are assumed to operate in a zenith-looking mode. As suggested by *Crewell and Löhnert* [2007], for HATPRO, we also include measurements at five different elevation angles in the analysis (Table 1).

[28] In order to combine different measurements from a set of various sensors, we make use of the optimal estimation theory [Rodgers, 2000]. This approach allows for a physically consistent retrieval of atmospheric state parameters. In this study, the atmospheric state vector \mathbf{x} consists of the vertical profiles of temperature and absolute humidity which are defined on 43 pressure levels ranging from 1013.25 hPa to 0.1 hPa. These profiles can be iteratively derived using the following optimal estimation equation:

$$\mathbf{x}_{i+1} = \mathbf{x}_i + (\mathbf{K}_i^T \mathbf{S}_e^{-1} \mathbf{K}_i + \mathbf{S}_a^{-1})^{-1} \times [\mathbf{K}_i^T \mathbf{S}_e^{-1} (\mathbf{y} - \mathbf{y}_i) + \mathbf{S}_a^{-1} (\mathbf{x}_a - \mathbf{x}_i)]. \quad (1)$$

[29] This 1D variational approach implies the knowledge of some a priori profile \mathbf{x}_a , as well as of the a priori and measurement/forward model uncertainties represented by the \mathbf{S}_a and \mathbf{S}_e covariance matrices, respectively. \mathbf{K} is the Jacobian, i.e., the sensitivity of the forward model \mathbf{F} with respect to changes in the atmospheric state. The observational vector \mathbf{y} includes the measurements from the different sensors. \mathbf{x}_i is the retrieved atmospheric state at the i th iteration step and $\mathbf{y}_i = \mathbf{F}(\mathbf{x}_i)$. In this study, different experiments with different measurement combinations are performed such that the vector \mathbf{y} may consist of different sets of ground- and/or satellite-based observations depending on the experiment configuration. The posterior error covariance matrix \mathbf{S} , which provides the estimated uncertainty of the most probable solution, is given by

$$\mathbf{S} = (\mathbf{K}^T \mathbf{S}_e^{-1} \mathbf{K} + \mathbf{S}_a^{-1})^{-1}. \quad (2)$$

[30] In order to quantify the information content of an observation in the retrieved atmospheric state, the number of degrees of freedom for signal (DOF) can be calculated. The DOF is the number of independent pieces of information that are determined from the measurements. It is given by the trace of the averaging kernel matrix \mathbf{A} :

$$\mathbf{A} = \mathbf{S} \cdot (\mathbf{K}^T \mathbf{S}_e^{-1} \mathbf{K}). \quad (3)$$

[31] Equation (1) is iterated until the value of \mathbf{x} converges. Since \mathbf{x} changes in each iteration step, also \mathbf{K}_i needs to be recalculated. The calculation of \mathbf{K} can be computationally very expensive especially when a large set of highly spectrally resolved measurements is included.

[32] In order to avoid this extensive application of forward model calculations, we followed the approach used in *Eyre* [1990]. Since the aim of this study is a first assessment of the benefit of different sensor combinations in T and q profiling, we used equations (2) and (3) but not the full retrieval framework. We performed the analysis for a variety of atmospheric situations using radiosonde T and q profiles. For each atmospheric profile, \mathbf{K} is calculated once by successively perturbing the temperature and absolute humidity profiles in each layer by 0.2 K and 1%, respectively. Since the primary focus of this study is the information content in the troposphere, we computed the Jacobians for all model layers below 20 km (~ 69 hPa).

[33] Given the Jacobian \mathbf{K} and well-defined \mathbf{S}_e and \mathbf{S}_a covariance matrices, the uncertainty of the retrieval and the DOF are estimated. In this way, the benefit of many different measurement combinations in many atmospheric conditions can be assessed without vast computational costs. Note that this approach implies the convergence of the retrieval to the true T and q profiles. Thus, our study is performed under optimum conditions. It has to be kept in mind that inaccurate representations of a priori, measurement, and forward model uncertainties may not lead to a convergence of equation (1). If the uncertainties in the prior profile and/or in the measurements were underestimated, the resulting retrieval uncertainties would be underestimated, too. Too small measurement uncertainties would also result in an overestimation of the information content of the measurements. This issue has also been addressed by *Aires* [2011], who pointed out that the synergy benefit is highly dependent on the hypotheses made in the retrieval. We also have to keep in mind that representativeness errors of the measurements are not included in the analysis and would, if taken into account, degrade the synergy benefit. However, with the hypotheses made in this study, i.e., ideal retrieval performance and horizontally homogeneous atmospheric conditions, we are able to assess the maximum benefit that can be achieved.

3.1. A Priori Information

[34] We performed the analysis for the Meteorological Observatory Lindenberg site [Neisser *et al.*, 2002] in Germany, which is located at 52.13°N and 14.07°E and thus characterized by a midlatitude, rather continental climate. The a priori covariance matrix was created using a quality controlled 8 year data set (1996–2003) of 6-hourly clear-sky radiosonde ascents. A radiosonde profile is assumed to be cloud-free if the relative humidity does not exceed 95% in any height level. The radiosonde data are interpolated to the 43 level pressure grid. Only those radiosondes are included which reached at least the 69 hPa pressure level. Standard atmospheric midlatitude summer and winter profiles are used to extend the T and q profiles up to 0.1 hPa, i.e., the highest model level. Since humidity measurements by radiosondes are reliable only up to 200–300 hPa, q profiles of the standard atmospheres are used for pressure levels above 200 hPa. In this way, a data set of 4854 radiosondes has been created which has been used

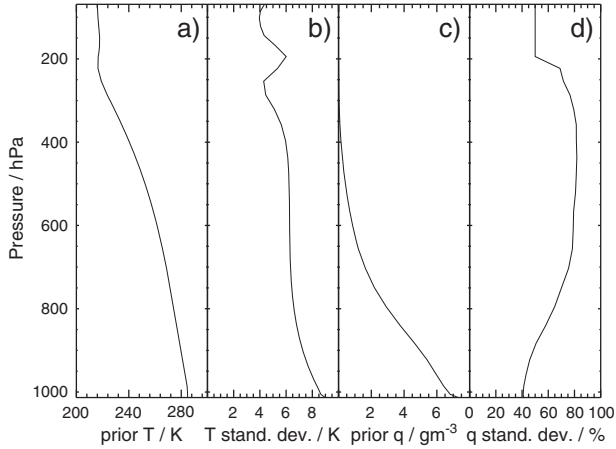


Figure 2. Eight-year (1996–2003) climatological mean profiles of (a) temperature (in K) and (c) absolute humidity (in g m^{-3}) and (b, d) corresponding standard deviations for Lindenberg, Germany. The mean profile was derived on the basis of 4854 clear-sky radiosonde ascents.

to derive a mean climatological profile as a priori profile (Figure 2a,c) and corresponding variances and covariances for \mathbf{S}_a which is given by

$$\mathbf{S}_a^{kj} = \text{CORR}(\mathbf{x}_k, \mathbf{x}_j) \sigma_{x_k} \sigma_{x_j}. \quad (4)$$

σ_{x_k} and σ_{x_j} are the standard deviations of the temperature or humidity at a certain height level k and j , respectively, and $\text{CORR}(\mathbf{x}_k, \mathbf{x}_j)$ the correlation between those two variables.

[35] The prior temperature uncertainty, which represents the variability of the T profiles at the Lindenberg site, clearly shows the tropopause region (Figure 2b). Due to the varying tropopause height during the year, the variance of the temperature shows a maximum around 200 hPa. The uncertainty of q is set to 50% at pressure levels above 200 hPa (Figure 2d). Since we assume standard T and q profiles above the 69 and 200 hPa levels, respectively, the inter-level correlation is set to zero in the corresponding height levels (Figure 3). Note that height levels above the 69 hPa level do not contribute to the calculated information content at all, since the corresponding entries in the Jacobian are zero. However, these levels are important in the forward model simulations: in order to model realistic observations, absorption and emission of the stratospheric height levels need to be taken into account. Excluding these heights could cause false sensitivities of the measurements to changes in the tropospheric profiles. In order to assess the sensitivity of the results with respect to the prior error covariance matrix, experiments with different uncertainty assumptions have been performed.

3.2. Forward Models

[36] In order to simulate the different sensor observations, appropriate forward models need to be applied (Table 1). For the highly spectrally resolved observations from the AERI and IASI instruments, we used the line-by-line radiative transfer model (LBLRTM) from the Atmospheric and Environmental Research Inc. [Clough *et al.*, 2005]. LBLRTM has been extensively validated, and its high accuracy allows the model to serve as a benchmark in the training of

fast radiative transfer codes [Delamere *et al.*, 2010; Turner *et al.*, 2004]. It has also been used for retrieval development with IASI [Shephard *et al.*, 2009] and AERI observations [Feltz *et al.*, 2003]. The version of the LBLRTM used in this work is LBLRTM_v11.6. The accuracy of LBLRTM is mainly determined by the uncertainties of the line parameters and the line shape. The uncertainties related to the spectroscopic parameters are in general about 5 times higher than those related to the computational procedures which are about 0.5% [Clough *et al.*, 2005]. In order to simulate realistic AERI and IASI observations, we also accounted for the corresponding resolution of the instrument and instrument response functions.

[37] SEVIRI radiances have been simulated with a very fast radiation transfer model (RTTOV), code version 9.3. RTTOV has been designed for passive IR and MW satellite radiometers, spectrometers, and interferometers. RTTOV has been originally developed at the ECMWF [Eyre, 1991] for TOVS (Tiros Operational Vertical Sounder). These days, the code is under development within the EUMETSAT NWP Satellite Application Facility (SAF), of which RTTOV-9 and RTTOV-10 are the latest versions [Saunders *et al.*, 1999, 2009]. The RTTOV transmittance scheme utilizes regression coefficients derived from line-by-line model calculations in order to express the optical depths as a linear combination of profile-dependent parameters. Since the regression coefficients have been determined for a specified vertical pressure grid, we use the same vertical grid as the retrieval grid in this study in order to avoid vertical interpolation of the temperature and humidity profiles. The accuracy of the RTTOV has been evaluated using line-by-line models and shows a strong dependency on the bandwidth of the channel and the presence of absorbers [Matricardi, 2009; Soden *et al.*, 2000]. Although RTTOV contains a Jacobian version of the model, we calculated \mathbf{K} using the finite differences method in order to make sure that for all instruments the Jacobians were calculated in the same way.

[38] Microwave synthetic observations have been calculated with the newly developed Passive and Active

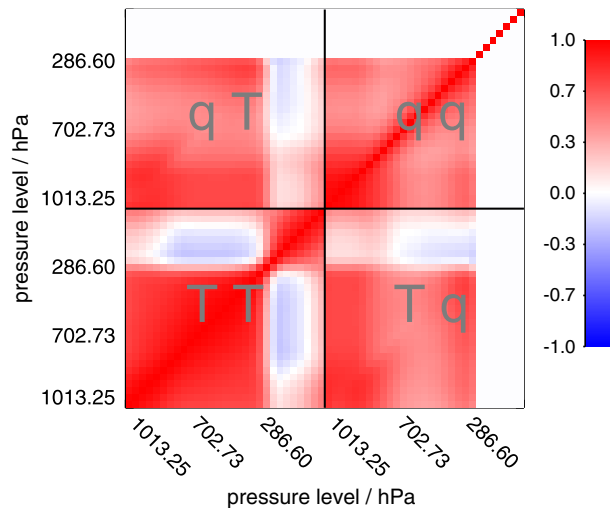


Figure 3. Correlation matrix for temperature and absolute humidity profiles derived from data of 4854 clear-sky radiosonde ascents at Lindenberg, Germany.

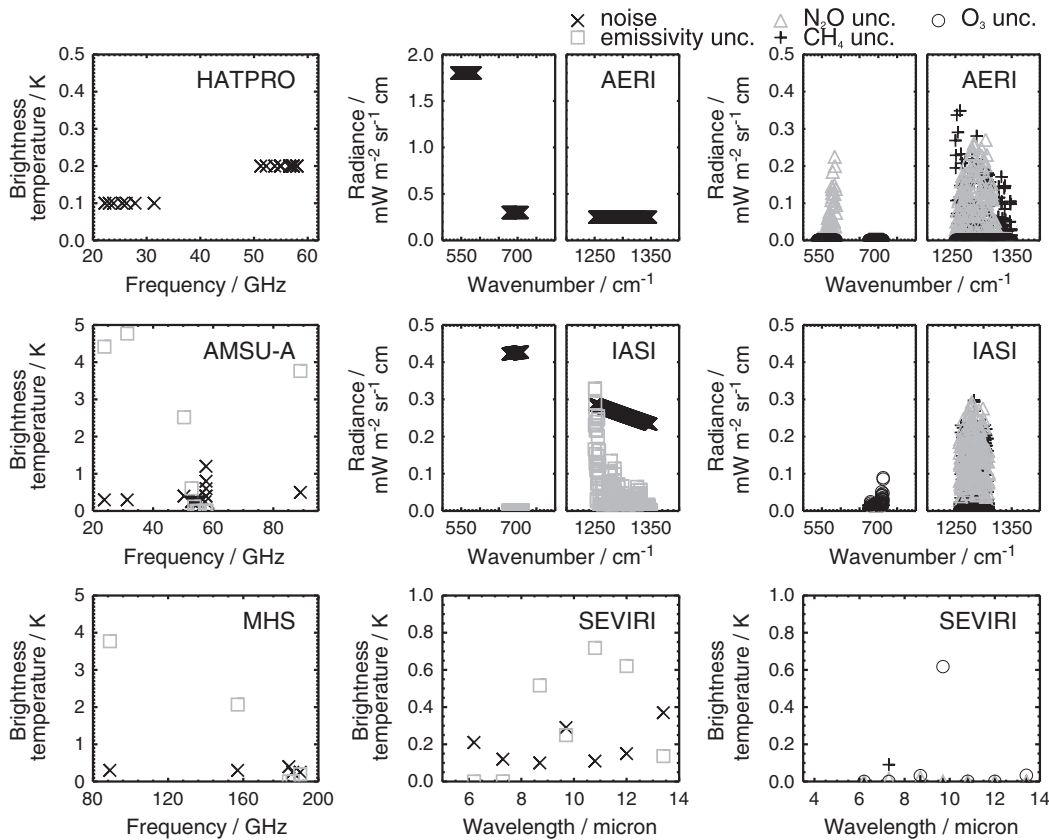


Figure 4. Measurement and forward model parameter uncertainties of the different sensors included in the study; (top left) HATPRO, (top center and top right) AERI, (middle left) AMSU-A, (middle center and middle right) IASI, (bottom left) MHS, (bottom center and bottom right) SEVIRI. Uncertainties due to instrument noise (black cross), surface emissivity (gray square), methane (black plus), nitrous oxide (gray triangle), and ozone (black circle).

Microwave Transfer model (PAMTRA), which uses methods as described in *Mech et al.* [2007] and applies the solution method as shown in *Evans and Stephens* [1995]. Absorption due to water vapor and oxygen are calculated using the Rosenkranz absorption model [*Rosenkranz*, 1998]. The Rosenkranz model has been modified to include the half width of the 22.2 GHz water vapor absorption line derived by *Liljegren et al.* [2005] and the adjusted strength of the foreign- and self-broadened water vapor continuum coefficients calculated by *Turner et al.* [2009].

3.3. S_e Matrix

[39] Measurement and forward model uncertainties are represented by the combined covariance matrix S_e . In this study, we use typical values of random instrument noise as measurement uncertainty (Figure 4 and section 2). For the AERI channels, we apply the same noise values as in the information content study by *Löhnert et al.* [2009]. Note that *Löhnert et al.* [2009] assumed larger uncertainties for the HATPRO channels since they took calibration uncertainties and random forward model uncertainties into account, too. The noise equivalent brightness temperatures of the IASI design specification (cf. section 2.5) have been transferred to uncertainties in terms of radiance units ($\text{mW m}^{-2} \text{sr}^{-1} \text{cm}$). All measurement errors are assumed to be uncorrelated, which makes S_e a diagonal matrix.

[40] In this study, we do not assume inherent forward model uncertainties, i.e., uncertainties related to the radiative transfer procedures themselves. As mentioned previously, the largest forward model uncertainties are related to the representation of the gaseous absorption, i.e., the absorption model used in the radiative transfer calculations. These uncertainties can be larger than the instrument noise and depend very much on the frequency [*Turner et al.*, 2009; *Hewison et al.*, 2006; *Cadeddu et al.*, 2007]. However, since we assume an optimal retrieval performance with an accurate forward model in order to assess the maximum synergy benefit, we do not account for these uncertainties in the analysis. Note that systematic uncertainties cannot be taken into account in this 1-D variational approach. Consequently, as for data assimilation in NWP models, any bias errors (e.g., in the measurements) need to be corrected for prior to the retrieval application.

[41] The simulated measurements are not only influenced by the retrieved temperature and humidity profiles but also by other forward model input parameters like surface temperature, surface emissivity, and trace gas profiles which are set to fixed values in this study. For the surface temperature, the temperature of the lowest atmospheric layer is assumed. Thus, uncertainties in these variables will lead to uncertainties in the simulated observations. Since we do not simultaneously derive these variables together

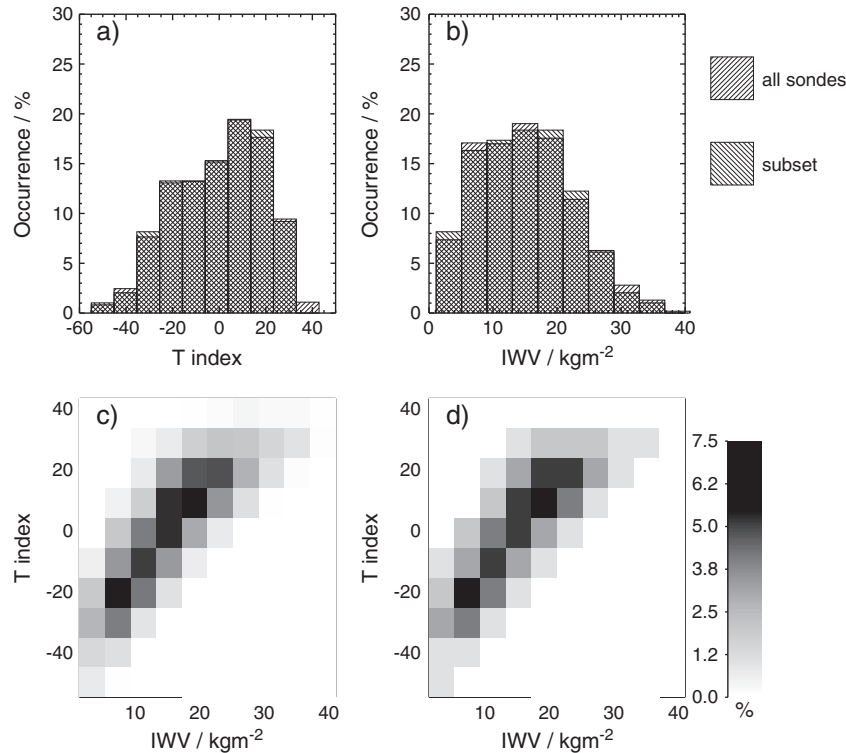


Figure 5. Histograms for (a) T_{index} and (b) IWV and joint probability histograms for (c) the whole profile data set and (d) the selected profile subset.

with the temperature and humidity profiles, corresponding uncertainty estimates need to be taken into account in the analysis. Typical uncertainties for the surface and trace gas properties are thus treated as forward model uncertainties and added to the measurement uncertainties in S_e .

[42] For the satellite observations, surface temperature and emissivity are critical parameters. The surface temperature is set to the temperature of the lowest model level. For the MWR frequencies, the surface emissivity has been derived for the Lindenberg site using land emissivity maps based on a precalculated monthly-mean emissivity climatology derived from Special Sensor Microwave/Imager (SSM/I) observations [Aires *et al.*, 2011b]. The accuracy of these emissivities is reported to be better than 2%. In our study, we use a fixed emissivity value for each AMSU-A/MHS channel which is the yearly mean of the monthly values. In order to get a realistic estimate of the surface emissivity for the IR observations, we used the MODIS emissivity product MOD11C3 for the Lindenberg pixel. As for the MWR channels, we calculated yearly mean values. Since MODIS does not provide measurements for the 6.2, 7.3, 9.7, and 13.4 μm channels, we applied the spectral dependence of emissivity for the vegetation type “leaf of old pine” from the MODIS USCB emissivity library to derive emissivities for the additional SEVIRI channels (MODIS University of California, Santa Barbara emissivity library available online at <http://www.ices.ucsb.edu/modis/EMIS/html/em.html>). Note that the exact emissivity values are not critical for this study since we perform the analysis on the basis of synthetic observations. We only want to assure that the assumed values are realistic. For the IASI observations, we simply set the emissivity to 0.99 for the wave numbers 675–713 cm^{-1} and to

0.97 for the wave numbers 1250–1350 cm^{-1} , which is in line with the SEVIRI channel emissivities. Calculations with these emissivities and with 2% decreased values have been performed for each of the 98 profiles in order to get an estimate for the forward model uncertainties of the surface parameters. Note that we only varied the emissivity and not surface temperature which would cause similar effects in the satellite observations.

[43] For the trace gas profiles, we used values of the standard midlatitude summer and winter profiles corresponding to the radiosonde dates. For the assessment of the corresponding forward model uncertainties due to unknown variations in the concentration, we focused on methane, ozone, and nitrous oxide being the prime trace gases in the IR spectrum. Note that the MW observations are not sensitive to the trace gas profiles. For each species, we successively applied a scaling factor of 0.95 to the whole profile in order to estimate the uncertainties in the ground-based and satellite IR observations. This 5% variation approximately complies with observed seasonal variations in total column amount of methane and nitrous oxide [Dils *et al.*, 2006].

[44] The uncertainties of surface emissivity and trace gas profiles have been accounted for in S_e using the mean difference of the simulated measurements for the perturbed and nonperturbed input parameters. As for the measurement noise, the uncertainties of the forward model are assumed to be uncorrelated. Note that in reality, these errors are expected to be strongly correlated between the channels which would increase the information coming from the measurements (since we constrain the measurement space) and decrease the retrieval uncertainties.

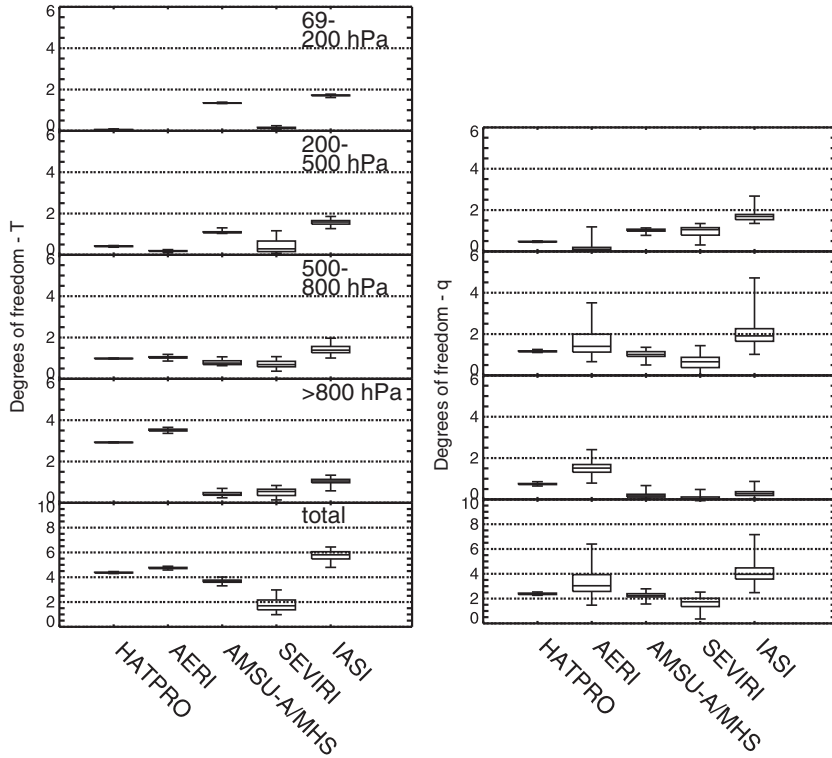


Figure 6. DOF for (left) temperature and (right) absolute humidity for retrievals including one sensor only. (line in box) Median, (box boundaries) 0.25 and 0.75 quantiles, and (whiskers) minimum and maximum values of the profile sample are shown.

[45] For AERI, methane and nitrous oxide contribute most to the forward model parameter uncertainties (Figure 4). For AMSU-A and MHS, the uncertainty in surface emissivity can be quite large especially for the window channels. The uncertainty in surface emissivity for the IASI wave numbers peaks along the wing of the water vapor absorption band around 1250 cm^{-1} . In contrast to AERI, IASI radiances show a sensitivity to the ozone concentration between 675 and 713 cm^{-1} . The magnitude of the methane and nitrous oxide forward model uncertainties is similar to AERI with maximum values of $0.3\text{ mW m}^{-2}\text{ sr}^{-1}\text{ cm}$. For SEVIRI, the emissivity uncertainty is especially pronounced in the $10.8\text{ }\mu\text{m}$, $12\text{ }\mu\text{m}$, and $8.7\text{ }\mu\text{m}$ channels. The largest uncertainty related to trace gases can be naturally found for ozone and the $9.7\text{ }\mu\text{m}$ ozone channel. Although the single values of the forward model uncertainties are typically smaller than the instrument noise, they can have a significant impact on the retrieval results and can generally not be neglected.

3.4. Selection of Profile Subset

[46] As presented in section 3, Jacobians are needed to evaluate the posterior error covariance matrix \mathbf{S} and the averaging kernel matrix \mathbf{A} . Since the calculation of the Jacobians is a computationally expensive process, the analysis is not performed for all 4854 available radiosondes but for a subset of about 100 profiles. In the profile selection process, we took care that the subset represents the interannual variability of the atmospheric conditions at Lindenberg. Because we are dealing with temperature and humidity profile retrievals, two indices were chosen to represent the statistical properties of the Lindenberg radiosonde

data set, namely, the integrated water vapor (IWV) and a temperature index (T_{index}) defined by

$$T_{\text{index}} = \sum_{z=0}^{12\text{km}} \frac{T(z) - \bar{T}(z)}{\sigma(z)}, \quad (5)$$

where $\bar{T}(z)$ and $\sigma(z)$ are the mean and the standard deviation for the vertical level z derived from all 4854 profiles. This temperature index was preferred to the temperature at ground or at a fixed altitude because it better represents the variability of the temperature profiles over the whole tropospheric column. The selection of the profile subset has been carried out trying to preserve the joint probability of IWV and T_{index} . In practice, the variability range of both the T_{index} and IWV was divided into 10 bins, resulting in a 10×10 bins matrix. For each of the 100 resulting bins, the fraction f of profiles belonging to that bin has been calculated. Then, $f \times 100$ profiles have been randomly extracted from all of the profiles associated with the corresponding bin. In this way, 98 profiles have been chosen which are analyzed in this study.

[47] This subset well reproduces the T_{index} and IWV statistic of the whole data set (Figure 5). For the joint probability histogram, the two data sets agree with a maximum difference among the bins of 0.6%.

4. Retrieval Uncertainty and Information Content Analysis

[48] We calculated the DOF and the estimated uncertainties in the T and q profiles for each of the selected 98 cases

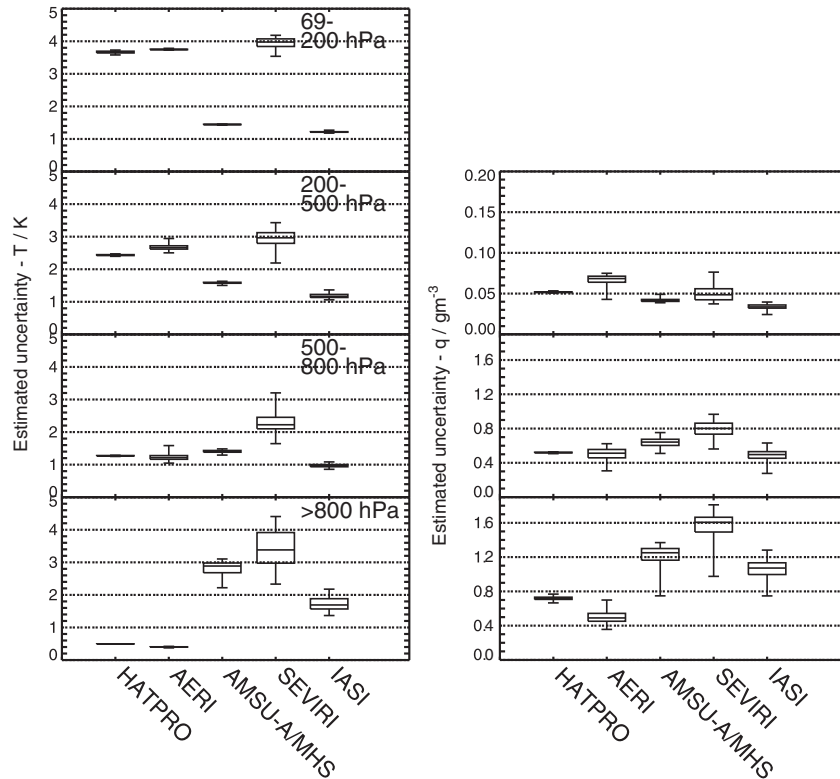


Figure 7. Estimated uncertainty of (left) temperature and (right) absolute humidity for retrievals including one sensor only. Median (line in box), 0.25 and 0.75 quantiles (box boundaries), and minimum and maximum values (whiskers) of the profile sample are shown.

and for different measurement combinations. The DOF and the uncertainties are analyzed for different height layers, i.e., 800–1013.25 hPa, 500–800 hPa, 200–500 hPa, and 69–200 hPa and for the whole atmospheric column, i.e., the total DOF. Since above 200 hPa the humidity of the standard midlatitude summer or winter atmosphere has been attached to each radiosonde profile and the corresponding entries in the Jacobian are the same for the 98 cases, we exclude these pressure layers in the analysis for the q profile. Unless noted otherwise, the DOF and uncertainty values discussed in the following are the median values of the 98 profiles.

4.1. Single Instruments

[49] Before analyzing the benefit of sensor synergy, we first examine the information content of a single instrument. In this way, the strengths and weaknesses of a retrieval using observations from one measurement platform only are assessed. These results also give a hint of where the measurements provide complementary information, and a distinct synergy benefit is thus expected. Starting with the baseline instrument, the ground-based MWR HATPRO provides 4.4 independent pieces of information for the T profile and 2.4 pieces of information for the q profile (Figure 6). For T , most of the information is located in the lowest height layer (67%), while the q DOF peaks between 500 and 800 hPa. About 89% and 79% of the T and q information, respectively, is from heights below the 500 hPa level. The accuracy of the profiles is best in the lowest height layer with 0.5 K for T and 0.72 gm^{-3} for q corresponding to a median

relative q uncertainty of 12% (Figure 7). In general, the accuracy is diminished with height resulting in a T uncertainty of 3.6 K above the 200 hPa level and in a q uncertainty of 59% for the 200–500 hPa layer.

[50] Concerning the DOF and the uncertainties in T and q , ground-based spectral IR observations from AERI outperform the HATPRO measurements in most height layers. For T , the total DOF of the AERI measurements are slightly larger (4.7). The total q DOF of the AERI shows a strong variability with a minimum (maximum) value of 1.5 (6.5) reflecting a high sensitivity to the atmospheric situation, which will be investigated in detail in section 4.3. With a median value of 3.0, the information content in q is larger by 0.6 compared to the corresponding value for HATPRO. The uncertainties of the T and q profiles of the AERI retrieval are in general smaller than those of the HATPRO retrieval, e.g., the median uncertainty of the humidity below the 800 hPa level is 0.49 gm^{-3} corresponding to a median relative uncertainty of 8%. However, the advantage of the AERI measurements is only restricted to height layers below the 500 hPa level. In the upper parts of the troposphere, the HATPRO retrieval performs slightly better (more DOF, smaller uncertainties) since the HATPRO water vapor channels are more transparent. The results of the HATPRO retrieval are hardly sensitive to the atmospheric situation in contrast to those of AERI (especially for humidity). This issue will be discussed in section 4.3.

[51] The satellite MW observations from AMSU-A and MHS provide 3.7 and 2.2 DOF in the T and q profiles,

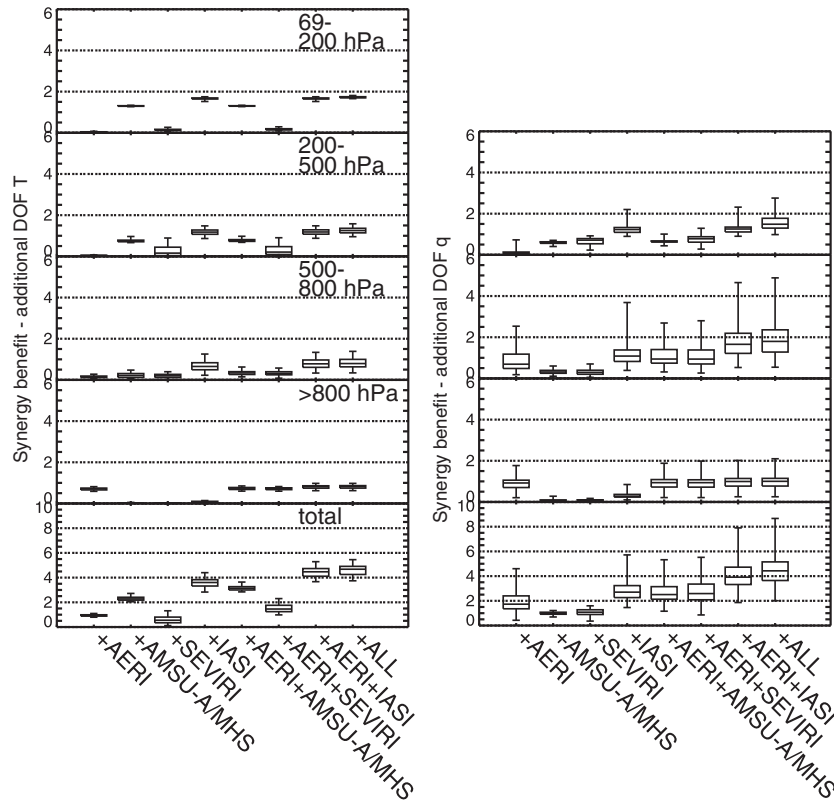


Figure 8. Synergy benefit in terms of additional DOF compared to HATPRO-only retrieval in the (left) temperature and (right) absolute humidity profile. Median (line in box), 0.25 and 0.75 quantiles (box boundaries), and minimum and maximum values (whiskers) of the profile sample are shown.

respectively, and thus 0.7 and 0.2 DOF less than the ground-based MWR observations. However, the potential of the AMSU-A and MHS measurements to complement the ground-based MWR observations is clearly visible for height layers above the 500 hPa level. There, the AMSU-A/MHS retrieval outperforms the HATPRO retrieval in terms of DOF and T and q uncertainties. Sixty-six percent and 46% of the satellite MWR T and q information, respectively, is from height layers above the 500 hPa level with corresponding T and q uncertainties of less than 1.6 K and 0.04 gm^{-3} (47%).

[52] The information content of the SEVIRI measurements with respect to temperature is smallest compared to the other observations. The total DOF is between 1.0 and 3.0 and stems primary from height layers between 200 and 800 hPa. Furthermore, the T uncertainties are quite large with a maximum accuracy of 2.2 K for the 500–800 hPa layer. However, the potential of the SEVIRI measurements for the humidity retrieval is better. Although still having the smallest total DOF compared to the other retrieval (1.7), SEVIRI can provide some information in the 200–500 hPa layer with a moderate uncertainty of 0.05 gm^{-3} (55%).

[53] In terms of DOF, the IASI retrieval outperforms the other ones (Figure 6). The temperature and humidity total DOF range from 4.8 to 6.4 and from 2.5 to 7.2, respectively, and thus show as the AERI measurements a high dependency on the atmospheric situation. Except for the lowest height layer, i.e., >800 hPa, where the ground-based instruments provide maximum information and smallest

uncertainties in T and q, the IASI retrieval performs best at all other pressure layers. The highest accuracy is achieved for the T and q profiles in the 500–800 hPa layer with uncertainties of 1.0 K in T and 0.50 gm^{-3} in q corresponding to a relative uncertainty in q of 18%. The accuracy of the IASI T retrieval is always better than 1.4 K above the 800 hPa level (Figure 7).

[54] From sensitivity experiments with and without forward model parameter uncertainties, it has been found that the effect of the variation of surface emissivity and trace gases on the DOF is small for temperature (not shown). The largest effect was found for the q DOF in case of AMSU-A/MHS, which is related to the high emissivity forward model uncertainties at the 23.8, 31.4, and 89 GHz channels. For AMSU-A/MHS, the q DOF would increase by 1.0 if S_e would include instrument noise only. In this case, the T and q DOF of the SEVIRI retrieval would increase by 0.5. For SEVIRI, this difference is primarily due to the surface emissivity uncertainty and to a small extent to the uncertainty of the ozone concentration. However, the forward model parameter uncertainties do have a noticeable impact on the estimated uncertainties in the T and q profiles, especially in the lowest pressure layer. About 17% and 22% of the T uncertainties of the AMSU-A/MHS and SEVIRI retrieval, respectively, are due to uncertainties of the forward model parameters. The corresponding values for the humidity uncertainty in the >800 hPa layer are 34% for AMSU-A/MHS and 21% for SEVIRI. For SEVIRI, the uncertainty of surface emissivity makes up about 85% of

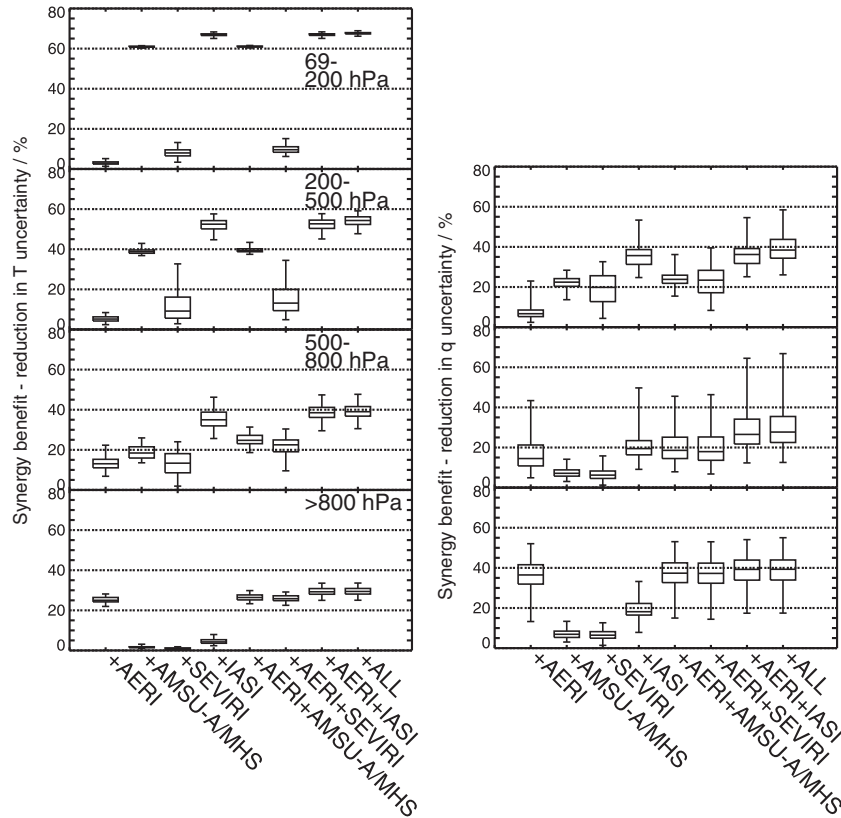


Figure 9. Synergy benefit in terms of reduction of uncertainty (in %) in (left) temperature and (right) absolute humidity compared to the HATPRO-only retrieval. Median (line in box), 0.25 and 0.75 quantiles (box boundaries), and minimum and maximum values (whiskers) of the profile sample are shown.

the forward model uncertainty followed by the contribution from the uncertainty in ozone concentration (11% for T, 6% for q). The emissivity and trace gas profile uncertainties do not have a noticeable effect on the IASI results.

4.2. Combined Instrumentation

[55] As mentioned before, the retrieval which includes the ground-based MWR observations only is regarded as the baseline retrieval in this study. The synergy benefit is therefore identified by relating the results of a combined instrument retrieval to those of the retrieval using HATPRO measurements only. Figure 8 depicts the additional DOF and Figure 9 the percentage reduction of the uncertainties in the retrieved T and q profiles, always with respect to the HATPRO-only retrieval. The results are shown for different instrument combinations. In addition, the synergy factor for DOF is summarized in Table 2. The synergy factor is defined as the ratio of the DOF for a retrieval including several instruments relative to the DOF for the HATPRO-only retrieval. Thus, a synergy factor of 1 means that there is no additional information to the HATPRO information.

[56] As expected from optimal estimation theory, the combination of HATPRO with one or more instruments always results in an increased number of DOF and in a reduction of the T and q uncertainty. First, the combination of HATPRO with one additional sensor will be discussed in detail followed by the analysis of the retrievals involving two or more instruments.

4.2.1. HATPRO With One Additional Instrument

[57] Combining HATPRO with AERI gives in total 0.9 and 1.7 additional DOF for the T and q profiles, respectively. This kind of measurement combination is beneficial for q in the 500–800 hPa layer and for T and q in the lowest height layer, where uncertainties can be reduced by 25% to 37%. Again, the synergy benefit for the q profile is strongly dependent on the atmospheric situation. The additional DOF, for example, varies between 0.4 minimum and 4.6 maximum and the synergy factor between 1.17 and 2.99. In some atmospheric situations, the uncertainty in q in the lowest height layer is even reduced by 52%.

[58] AMSU-A/MHS measurements significantly improve the T information with additional 2.3 DOF, i.e., about 50%

Table 2. Synergy Factor for Different Instrument Combinations^a

Instruments: HATPRO+	Synergy Factor					
	Temperature			Humidity		
	Min	Max	Median	Min	Max	Median
AERI	1.18	1.25	1.22	1.17	2.99	1.74
AMSU-A/MHS	1.46	1.63	1.52	1.28	1.52	1.42
SEVIRI	1.03	1.13	1.30	1.15	1.68	1.45
IASI	1.64	2.02	1.82	1.64	3.37	2.13
AERI+AMSU-A/MHS	1.65	1.83	1.72	1.48	3.31	2.07
AERI+SEVIRI	1.22	1.53	1.34	1.35	3.39	2.09
AERI+IASI	1.83	2.22	2.02	1.76	4.27	2.63
ALL	1.85	2.26	2.06	1.83	4.59	2.84

^aThe synergy factor is defined as the ratio of the DOF of a certain retrieval compared to the DOF of the HATPRO-only retrieval.

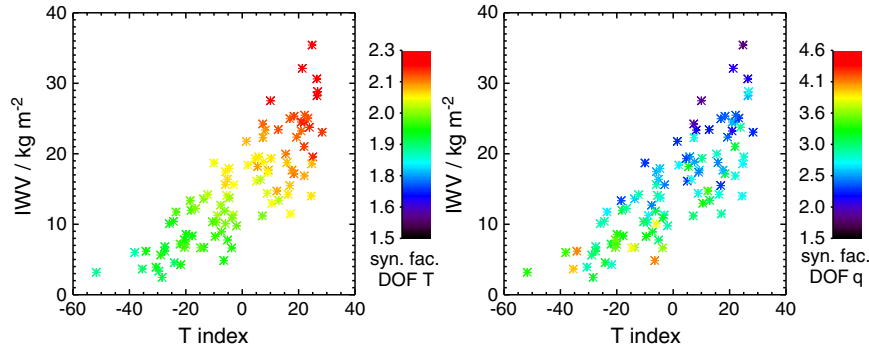


Figure 10. (left) Temperature and (right) absolute humidity synergy factor for a retrieval including all measurements as a function of the T index and the IWV.

of the HATPRO DOF, which are primarily from height layers above the 500 hPa level. For the upper T profile, the uncertainty is reduced by up to 60%. For q , the AMSU-A/MHS observations are less beneficial. The total DOF increases by 1.0. Maximally, 50% of the HATPRO q DOF are added by the AMSU-A/MHS observations. The maximum improvement of the q uncertainty (22%) can be found for the 200–500 hPa layer.

[59] As seen for the single instrument retrieval, SEVIRI's information on the T and q profiles is smaller compared to the other instruments. Additional information on T and q is available especially for the 200–800 hPa layers, where uncertainties can be reduced by up to 10% (T) and 20% (q). In total, the additional DOF are 0.6 for T and 1.1 for q and the synergy factor typically about 1.1 and 1.5 for T and q , respectively. For the humidity profile, the inclusion of SEVIRI observations therefore yields similar results as for the inclusion of the AMSU-A/MHS channels.

[60] With the highly spectrally resolved IR observations, IASI can substantially increase the measurement information and decrease the uncertainties for height layers above the 800 hPa level. The total DOF increase by 3.6 and 2.7 for T and q , respectively. While the T DOF can be maximally doubled, the q DOF can even be more than tripled. The temperature uncertainty in the upper layers is reduced by 68% (<200 hPa) and 53% (200–500 hPa). The humidity uncertainty can be improved by 25% to 53% in the uppermost tropospheric layer.

4.2.2. HATPRO With Two and More Additional Instruments

[61] In the following, the advantage of the combination of HATPRO with measurements of two other instruments is discussed. If ground-based spectrally IR observations are available, it is convenient to combine the information of both ground-based instruments, HATPRO and AERI, in order to improve the estimates of T and q in the troposphere. The combination with one satellite sensor can further improve the profiles in the middle and upper tropospheric layers.

[62] If the HATPRO measurements are combined with AERI and IASI, the total DOF in the T and q profiles are increased by 4.5 and 4.0, respectively, where the additional information is distributed throughout the whole atmospheric profile. The uncertainties in the different layers are reduced by 30% to 68% for T and by 25% to 40% for q . As the spectrally IR observations are included, the synergy benefit reveals a high variability among the 98 atmospheric cases,

especially for humidity. The synergy factor varies from 1.83 to 2.22 for T and from 1.76 to 4.27 for q .

[63] Combining HATPRO with AERI and AMSU-A/MHS is less beneficial than the combination with AERI and IASI. Compared to the HATPRO-only retrieval, the DOF increase by 3.2 (T) and 2.5 (q). Uncertainties in T can be diminished by 25% (lower troposphere) to 60% (upper troposphere), and uncertainties in q by 18% and 38%.

[64] If HATPRO, AERI, and SEVIRI are combined, the synergy benefit is dominated by the benefit of the AERI measurements. The additional DOF for T (q) range between 1.0 and 2.4 (1.0 and 5.5) with a median value of 1.5 (2.5). While in the upper height layers, the uncertainty in T and q can further be decreased if SEVIRI measurements are added to the AERI observations, the improvement in the uncertainty in the lowest height layer is only due to the AERI measurements.

[65] For these three instrument combinations, it is found that synergy benefit in terms of additional DOF is roughly the sum of the additional DOF of a single instrument (see section 4.2.1). Thus, the information of the sensors seems to be quite complementary. Note that this additive synergy benefit is not apparent with respect to the estimated T and q uncertainties.

[66] Combining all sensors used in this study results in the largest information content and smallest T and q uncertainties. However, the differences in DOF and uncertainties compared to the combined HATPRO-AERI-IASI retrieval are very small showing that AMSU-A/MHS and SEVIRI can hardly add complementary information in cloud-free conditions.

4.3. Sensitivity to Atmospheric Conditions

[67] Figures 8 and 9 and Table 2 clearly show that the synergy benefit can be quite different in different atmospheric conditions. In order to assess this sensitivity, Figure 10 depicts the synergy factor for the T and q DOF of the retrieval including all sensors as a function of the temperature index (equation (5)) and the IWV. Note that the HATPRO retrieval is rather insensitive to changes in the atmospheric conditions with DOF for T and q of 4.4 and 2.4, respectively. Thus, variations in the synergy factor are related to variations in the DOF of the other instrumentation.

[68] For temperature, the synergy factor increases with increasing temperature and/or increasing humidity resulting in a Spearman's rank correlation coefficient of 0.90 and

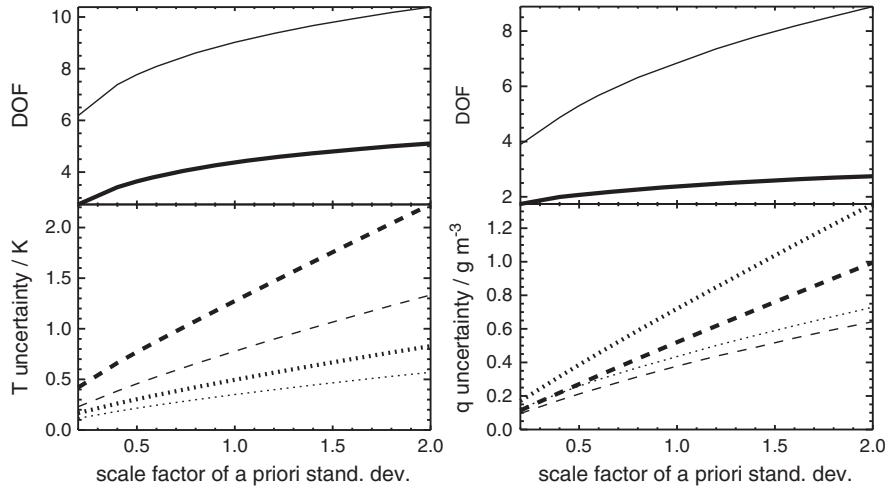


Figure 11. (top) Total DOF and (bottom) estimated uncertainties for (left) temperature and (right) absolute humidity as a function of the prior uncertainty. The values reported are the median values of the 98 profiles for a retrieval using HATPRO only (thick lines) and a retrieval using all instruments (thin lines). The uncertainties are layer mean values for 200–500 hPa (dashed) and >800 hPa (dotted).

0.96 for the temperature index and the IWV, respectively. In cold and dry situations, the minimum value of the synergy factor is 1.85, while in warm and humid conditions, the DOF are maximally increased by a factor of 2.26 (see also Table 2) compared to a retrieval with ground-based MWR observations only.

[69] For the humidity profile, the synergy factor is negatively correlated with the IWV and with the temperature index where the correlation is more pronounced for humidity (-0.63) than for temperature (-0.47). Note that temperature and humidity are not independent from each other (cf. Figure 5) and that a higher IWV often goes along with a higher temperature (correlation of 0.84). The synergy factor for the humidity profile is much more variable than for the temperature profile with a value of down to 1.85 in humid atmospheric conditions and a value of up to 4.59 in dry situations.

[70] Note that the magnitude of the variations in the synergy factor is primarily determined by the strong variability of the humidity Jacobian of the IR observations (Table 2), in particular of the IR water vapor channels. For AERI, the channels at the $18 \mu\text{m}$ H_2O absorption band ($538\text{--}588 \text{ cm}^{-1}$) become more and more saturated. Compared to dry situations, the AERI measurements are therefore less sensitive to small changes in q and provide less information on the humidity profile. In conjunction with the observed moisture variability in Lindenberg, this results in the strong variability of the synergy factor. The variability of the synergy factor for the IASI retrieval is due to a combined effect, i.e., the raise of the height of the weighting functions in humid conditions and the variability of the prior uncertainty with height. It has to be noted that the variability of the synergy factor for the humidity profile in the combined HATPRO-AMSU-A/MHS retrieval is due to the MHS observations only, to be exact due to the 184 and 186 GHz channels which are most sensitive to changes in q in cold and dry situations.

[71] While the variation in the synergy factor concerning the humidity profile is qualitatively the same for the different instruments, the sensitivity of the synergy factor

for T varies among the instruments (not shown): for IASI and AMSU-A/MHS, the variation in the T synergy factor is qualitatively the same as for the retrieval which includes all measurements, i.e., a higher synergy factor with increasing temperature and/or increasing humidity. This is related to a higher sensitivity of most of the channels in warm and humid conditions. In these situations, the increased opacity leads to an improved resolution of the IASI and AMSU-A/MHS temperature profiles. For AERI, there is a positive correlation with temperature of 0.47 resulting from a higher sensitivity of all wave number bands in warmer situations. However, there is rather no dependency on humidity. In fact, the small correlation with the IWV of 0.20 is due to the correlation of the T and q profiles accounted for in S_a .

4.4. Sensitivity to A Priori Accuracy

[72] In order to assess the sensitivity of the synergy benefit with respect to the a priori accuracy, an experiment has been performed in which the prior temperature and humidity standard deviations (cf. Figures 2b and 2d) are modified by applying different scaling factors from 0.2 to 2.0 to $\sigma_{x_{kj}}$ in equation (4). This has an effect on the variances and covariances in S_a corresponding to a scaling factor for S_a between 0.04 and 4. Note that smaller variances most likely go along with smaller correlations as it is the case for background covariance matrices used in NWP. However, in this study, the interlevel correlation is not changed in order to keep the interpretation of the results simple.

[73] The resulting total DOF for T and q and the corresponding estimated retrieval uncertainties in different height layers are exemplarily shown for the HATPRO-only retrieval and the retrieval including all sensors (Figure 11). Increasing the prior uncertainty leads to an increased number of total DOF. For the combined retrieval, doubling the prior uncertainty results in additional 1.4 and 2.1 DOF for T and q corresponding to an increase of 16% and 31%, respectively. The DOF for the HATPRO-only retrieval increase by 0.8 (19%) for T and by 0.3 (12%) for q . Thus, more information in the temperature and humidity profiles comes from

the measurements since the weight in the retrieval is shifted from the a priori information to the observations.

[74] The increase in DOF due to the increase of the prior uncertainty goes along with an increase of the estimated uncertainties for the T and q profiles. In case of a doubling of the prior uncertainty, for example, the mean T uncertainty in the lowest layer is raised by about 0.3 K for both retrievals and about 1 K (0.6 K) in the 500–800 hPa layer for the HATPRO-only (all instrument) retrieval. For humidity, the estimated uncertainty of the HATPRO-only retrieval is roughly doubled, while the relative increase in the uncertainty of the combined retrieval is smaller, i.e., around 70%.

[75] Since the vertical profile information of the measurements is limited, the DOF asymptotically approach a maximum DOF with increasing a priori uncertainty. For the HATPRO-only retrieval, this threshold value is about 9 for the temperature and 4 for the humidity profile if no a priori information is given, i.e., if the a priori uncertainty is set to a very large value (not shown). The corresponding maximum DOF from the overall combined ground- and satellite-based instruments retrieval are around 20. However, the associated, tremendous T and q uncertainties make the profile information useless in this case. Thus, when assessing the information content, it is always indispensable to analyze the DOF in conjunction with the estimated profile uncertainties.

[76] Interestingly, the synergy factor, i.e., the ratio of the DOF for the combined retrieval and the DOF for the HATPRO-only retrieval, is rather independent from the a priori accuracy in case for the temperature profile (not shown). For humidity however, the synergy factor slightly increases from about 2.8 (cf. Table 2) to 3.2 if the prior uncertainty is doubled. In this case, the sensor synergy is thus even more valuable.

[77] If T and q profiles from operational NWP models would be used as a priori information, the uncertainties of the prior profiles would be much smaller compared to the corresponding climatological ones. If typical accuracies of about 1 K for temperature and 10% for humidity are assumed, the corresponding scaling factor for S_a is about 0.2. In this case, the additional DOF compared to the HATPRO retrieval are 2.3 and 2.2 for T and q, respectively, which corresponds to a factor of 2.2 of the HATPRO DOF. In terms of accuracy improvement, the additional instruments reduce the T uncertainty by about 32%, 45%, and 45% in the lower, middle, and upper troposphere, respectively. The corresponding values for the humidity are 27%, 15%, and 35%.

5. Discussion and Outlook

[78] In this paper, we analyzed the synergy benefit of ground-based and satellite MWR and IR observations in the retrieval of tropospheric temperature and humidity clear-sky profiles for a midlatitude site. It is assumed that climatological mean T and q profiles are available for the site and are used as a priori information. On this basis, it has been shown that passive ground-based MW radiometry provides about 4.4 and 2.4 independent pieces of information for the temperature and humidity profiles, respectively. Similar num-

bers have been found by *Löhnert et al.* [2009] for another central European site. For T profiling, the inclusion of IASI and AMSU-A/MHS is very beneficial with a multiplicative factor of the DOF of about 1.8 and 1.5, respectively. For the humidity profile, IASI and AERI can substantially increase the information compared to the ground-based MWR observations. For IASI, for example, the DOF are more than doubled. The additional measurements not only increase the vertical profile information but also enhance the accuracy with smaller estimated uncertainties in T and q.

[79] A closer look reveals that the AERI observations are essential in order to improve the profile information in the lower troposphere, i.e., more DOF and a better profile accuracy. However, at most ground-based stations which are equipped with a MWR, AERI observations are not available [*Hardesty et al.*, 2012]. Thus, the combination of HATPRO with satellite information is more likely. IASI significantly improves the profile information in the middle and upper troposphere for both temperature and humidity, while AMSU-A/MHS provides valuable information for T above 500 hPa. Although less beneficial than the other sensors, SEVIRI can provide some additional information especially for upper tropospheric humidity. The increase in DOF for q of about 50% compared to the ground-based MWR retrieval goes along with a reduction in the humidity uncertainty by up to 20%. Even if the synergy benefit is less pronounced for SEVIRI, the advantage of SEVIRI is the higher temporal and spatial resolution of the measurements compared to IASI and AMSU-A/MHS. This makes a combined ground-based/satellite retrieval more feasible for the geostationary observations. With the future launch of the Meteosat Third Generation satellite, the limited capability of SEVIRI to provide T and q information is remedied, since then in addition, highly spectrally resolved long-wave IR and midwave IR observations will be provided by the geostationary platform. The Infrared Sounder (IS) instrument will deliver 1720 channels with a spatial resolution of 4 km. Since the experimental framework used in this study is very flexible concerning further instruments and channels, the synergy analysis could be easily extended for the IS specifications.

[80] In case that all instruments, i.e., HATPRO, AERI, AMSU-A/MHS, SEVIRI, and IASI, are combined, the profile information on temperature is doubled and the information on humidity nearly tripled, which is particularly due to the highly spectrally resolved IR ground-based and satellite observations. T and q uncertainties in the lowest height layer can be reduced by 30% (T) and 40% (q), between 200 and 500 hPa even by 55% and 40%, respectively.

[81] Although we started the analysis from a ground-based perspective, the synergy benefit could also be assessed from a satellite point of view: given the IASI observations, how does ground-based instrumentation improve the T and q profiles? Compared to a IASI-only retrieval, for example, the inclusion of HATPRO or AERI measurements can significantly improve the thermodynamic profiles in the lower troposphere. While HATPRO increases the DOF in the lowest height layer by a factor of 2.8 and 3.6 for T and q, respectively, the corresponding values for AERI are with 3.5 and 6.0 even higher.

[82] The results of this study showed that, especially for the humidity profile and the spectral IR observations, the

synergy benefit is highly dependent on the atmospheric situation, in particular on the integrated water vapor. In moister conditions, the AERI IR water vapor channels become more opaque and less sensitive to changes in q or even saturated. Thus, their potential to add information on the height profile is reduced. It has to be noted that therefore the results of this study are only valid for this climatic regime and may change if the analysis is shifted to a different site. Löhnert *et al.* [2009], for example, showed that, for a tropical climate, the information content of the IR observations is much less than for the climate of a central European site.

[83] It has to be pointed out that the synergy benefit, i.e., the additional DOF and the reduction in uncertainty, is quite sensitive to the error assumptions made. Since we did not account for, e.g., calibration uncertainties, uncertainties due to the forward models themselves, and representativeness uncertainties due to different fields of view, the uncertainties in S_e would be generally higher. Together with a mean climatic profile as a priori and thus with a quite uncertain a priori information, the estimated DOF and the accuracy in T and q presented in this study are at the high end of the expected synergy benefit. As seen from the sensitivity studies, the synergy benefit in terms of additional DOF would likely be smaller if the prior profiles would be known better, e.g., if T and q profiles from NWP would be used. The fact that we did not include surface temperature and emissivity in the atmospheric state vector might also affect the results. In clear-sky conditions, satellite observations at atmospheric window frequencies are dominated by the signal from surface emission. Since the surface temperature is most probably correlated to T and q of adjacent atmospheric layers, these window channels can indirectly provide information on the atmospheric profiles in the lower troposphere. However, some first tests with an extended atmospheric state vector now including surface temperature (not shown) did not alter the main conclusions presented in this study.

[84] The sensitivity of the synergy benefit to S_a and S_e has also been addressed by Aires [2011]. He suggests to measure synergy by directly comparing the retrieval results to the true profiles if synthetic data are used in order to obtain realistic estimates of the retrieval uncertainties and in this respect the synergy benefit. Since the theoretical considerations of our study provided an upper limit of what can be expected by combining the different sensors, in a next step, we will apply the full retrieval and test if the estimated uncertainties in T and q are consistent with the true errors in the retrieved profiles.

[85] In this context, it is necessary to reduce the size of the measurement vector in order to make the full retrieval feasible, i.e., with reasonable computational costs. Especially for the highly spectrally resolved IR observations, the channel selection needs to be optimized, e.g., as in Merrelli and Turner [2012]. Another possibility is to use compression techniques for the spectral information like the principal component analysis [Aires *et al.*, 2011a]. Of course, this modification has an effect on the synergy benefit, too, and needs to be assessed.

[86] The assumption of horizontally homogeneous conditions for temperature and humidity in the instruments' field of view might be not too far from reality in clear-sky cases. However, as soon as it comes to cloudy cases and real measurements, the spatial and temporal representativeness of

the measurements is an important issue which needs to be assessed. In ongoing studies, we analyze the ground-based and satellite synergy in the retrieval of cloud properties. This study will then include passive and active instrumentation. We will also simulate the microwave package on board the German High Altitude Long Range research aircraft (HALO) composed of a 26-channel MWR and a 36 GHz cloud radar. Because of the similar fields of view of the HAMP (HALO Microwave Package) instruments from about 12 km height and the ground-based ones, the assumption that all sensors see the same scene is still reasonable. In the cloudy cases, observations from down looking radiometers are probably more beneficial for the T and q profiles than the IR ones, since the IR observations become quickly saturated and have only limited profile information.

[87] **Acknowledgments.** This work has been funded by the German Research Foundation within the project ICOS—Integrating Cloud Observations from Ground and Space under grant CR111/8-1 and the project Using the HALO Microwave Package (HAMP) for cloud and precipitation research under grant CR111/9-1. We acknowledge the German Weather Service for providing the radiosonde data. Furthermore, the authors thank Dr. David D. Turner for assisting in the radiative transfer calculations and for his valuable suggestions which helped to improve the manuscript. The comments from three anonymous reviewers also improved the clarity of the manuscript and are gratefully acknowledged.

References

- Aires, F. (2011), Measure and exploitation of multisensor and multi-wavelength synergy for remote sensing: 1. Theoretical considerations, *J. Geophys. Res.*, *116*, D02301, doi:10.1029/2010JD014701.
- Aires, F., M. Paul, C. Prigent, B. Rommen, and M. Bouver (2011a), Measure and exploitation of multisensor and multiwavelength synergy for remote sensing: 2. Application to the retrieval of atmospheric temperature and water vapor from MetOp, *J. Geophys. Res.*, *116*, D02301, doi:10.1029/2010JD014702.
- Aires, F., C. Prigent, F. Bernardo, C. Jiménez, R. Saunders, and P. Brunel (2011b), A Tool to Estimate Land-Surface Emissivities at Microwave frequencies (TELSEM) for use in numerical weather prediction, *Q. J. R. Meteorol. Soc.*, *137*, 690–699.
- Aires, F., O. Aznay, C. Prigent, M. Paul, and F. Bernardo (2012), Synergistic multi-wavelength remote sensing versus a posteriori combination of retrieved products: Application for the retrieval of atmospheric profiles using MetOp-A, *J. Geophys. Res.*, *117*, D18304, doi:10.1029/2011JD017188.
- Cadeddu, M. P., V. H. Payne, K. Cady-Pereira, and J. C. Liljegren (2007), Effect of the oxygen line-parameter modeling on temperature and humidity retrievals from ground-based microwave radiometers, *IEEE Trans. Geosci. Remote Sens.*, *45*, 2216–2223.
- Cardinali, C., (2009), Forecast sensitivity to observation (FSO) as a diagnostic tool, *Tech. Rep.*, 599, European Centre for Medium Range Weather Forecasts Shinfield Park, Reading, Berkshire RG2 9AX, England, [Available at http://www.ecmwf.int/publications/library/ecpublications/_pdf/tm/501-600/tm599.pdf].
- Chalon, G., F. Cayla, and D. Diebel (2001), IASI—An advanced sounder for operational meteorology, paper presented at 52nd International Astronautical Federation, Toulouse, France.
- Clough, S. A., M. W. Shephard, E. J. Mlawer, J. S. Delamere, M. J. Iacono, K. Cady-Pereira, S. Boukabara, and P. D. Brown (2005), Atmospheric radiative transfer modeling: A summary of the AER codes, Short Communication, *J. Quant. Spectrosc. Radiat. Transfer*, *91*, 233–244.
- Crewell, S., and U. Löhnert (2007), Accuracy of boundary layer temperature profiles retrieved with multi-frequency, multi-angle microwave radiometry, *IEEE Trans. Geosci. Remote Sens.*, *45*(7), 2195–2201.
- Delamere, J. S., S. A. Clough, V. Payne, D. D. Turner, and R. Gamache (2010), A far-infrared radiative closure study in the Arctic: Application to water vapor, *J. Geophys. Res.*, *115*, D17106, doi:10.1029/2009JD012968.
- Dils, B., et al. (2006), Comparisons between SCIAMACHY and ground-based FTIR data for total columns of CO, CH₂, CO₂ and N₂O, *Atmos. Chem. Phys.*, *6*, 1953–1976.
- EUMETSAT (2012), *IASI Level 1 Product Guide*, Eumetsat-Allee 1, D-64295 Darmstadt, Germany. [Available at http://www.eumetsat.int/groups/ops/documents/document/pdf_iasi_level_1_prod_guide.pdf].

- Evans, K., and G. Stephens (1995), Microwave radiative transfer through clouds composed of realistically shaped ice crystals. Part I: Single scattering properties, *J. Atmos. Sci.*, *52*(11), 2041–2057.
- Eyre, J. R. (1990), The information content of data from satellite sounding systems: A simulation study, *Q. J. R. Meteorol. Soc.*, *116*, 401–434.
- Eyre, J. R. (1991), A fast radiative transfer model for satellite sounding systems, *Tech. Rep.*, 176, European Centre for Medium Range Weather Forecasts Shinfield Park, Reading, Berkshire RG2 9AX, England, [Available at http://www.ecmwf.int/publications/library/ecpublications/_pdf/tm/001-300/tm176.pdf].
- Feltz, W. F., W. L. Smith, R. O. Knuteson, H. E. Revercomb, and H. B. Howell (1998), Meteorological applications of temperature and water vapor retrievals from the ground-based Atmospheric Emitted Radiance Interferometer (AERI), *J. Appl. Meteorol.*, *37*, 857–875.
- Feltz, W. F., H. B. Howell, R. O. Knuteson, H. Woolf, and H. E. Revercomb (2003), Near-continuous profiling of temperature, moisture, and atmospheric stability using the Atmospheric Emitted Radiance Interferometer (AERI), *J. Appl. Meteorol.*, *42*, 584–597.
- Güldner, J., and D. Spänkuch (2001), Remote sensing of the thermodynamic state of the atmospheric boundary layer by ground-based microwave radiometry, *J. Atmos. Oceanic Technol.*, *18*, 925–933.
- Hardesty, R. M., et al., (2012), Thermodynamic profiling technologies workshop report to the National Science Foundation and the National Weather Service, *NCAR Tech. Rep.*, *NCAR/TN-488+STR*, Natl. Cent. for Atmos. Res., Boulder, Colo, [Available at <http://nldr.library.ucar.edu/repository/assets/technotes/TECH-NOTE-000-000-000-853.pdf>].
- Hewison, T. (2007), 1D-VAR retrieval of temperature and humidity profiles from a ground-based microwave radiometer, *IEEE Trans. Geosci. Remote Sens.*, *45*(7), 2161–2168, doi:10.1109/TGRS.2007.898,091.
- Hewison, T., D. Cimini, L. Martin, C. Gaffard, and J. Nash (2006), Validating clear air absorption models using ground-based microwave radiometers and vice-versa, *Meteorol. Z.*, *15*, 27–36.
- Hilton, F., et al. (2012), Hyperspectral Earth observation from IASI: Five years of accomplishments, *Bull. Am. Meteorol. Soc.*, *18*, 347–370.
- Klaes, K., et al. (2007), An introduction to the EUMETSAT polar system, *Bull. Am. Meteorol. Soc.*, *88*(7), 1085–1096.
- Knuteson, R. O., et al. (2004a), Atmospheric Emitted Radiance Interferometer. Part I: Instrument design, *J. Atmos. Oceanic Technol.*, *21*, 1763–1776.
- Knuteson, R. O., et al. (2004b), Atmospheric Emitted Radiance Interferometer. Part II: Instrument performance, *J. Atmos. Oceanic Technol.*, *21*, 1777–1789.
- Liljegren, J., S. Boukabara, K. Cady-Pereira, and S. Clough (2005), The effect of the half-width of the 22-GHz water vapor line on retrievals of temperature and water vapor profiles with a 12-channel microwave radiometer, *IEEE Trans. Geosci. Remote Sens.*, *43*(5), 1102–1108.
- Löhnert, U., and O. Maier (2012), Operational profiling of temperature using ground-based microwave radiometry at Payerne: Prospects and challenges, *Atmos. Meas. Tech.*, *5*, 1121–1134.
- Löhnert, U., D. D. Turner, and S. Crewell (2009), Ground-based temperature and humidity profiling using spectral infrared and microwave observations. Part I: Simulated retrieval performance in clear-sky conditions, *J. Appl. Meteorol.*, *48*, 1017–1032.
- Matricardi, M. (2009), An assessment of the accuracy of the RTTOV fast radiative transfer model using IASI data, *Atmos. Chem. Phys.*, *9*, 9491–9535.
- Mech, M., S. Crewell, I. Meirold-Mautner, C. Prigent, and J.-P. Chaboureaud (2007), Information content of millimeter observations for hydrometeor properties in mid-latitudes, *IEEE Trans. Geosci. Remote Sens.*, *45*(7), 2287–2299, doi:10.1109/TGRS.2007.898,261.
- Merrelli, A., and D. D. Turner (2012), Comparing information content of upwelling far-infrared and midinfrared radiance spectra for clear atmosphere profiling, *J. Atmos. Oceanic Technol.*, *29*, 510–526.
- Neisser, J., W. Adam, F. Beyrich, U. Leiterer, and H. Steinhagen (2002), Atmospheric boundary layer monitoring at the meteorological observatory Lindenberg as a part of the Lindenberg column: Facilities and selected results, *Meteorol. Z.*, *11*, 241–253.
- NOAA (2009), *NOAA KLM User's Guide (February 2009 revision)*, U.S. Department of Commerce National Oceanic and Atmospheric Administration National Environmental Satellite, Data, and Information Service, 151 Patton Avenue, Asheville, North Carolina, USA. [Available at <http://www.ncdc.noaa.gov/oa/pod-guide/ncdc/docs/klm/html/c3/sec3-9.htm>].
- Radiometer Physics GmbH, (2011), Technical instrument manual, *Tech. Rep.*, Birkenmaarstraße 10 53340, Meckenheim, Germany, [Available at http://www.radiometer-physics.de/rpg/html/docs/RPG_MWR_STD_Technical_Manual.pdf].
- Rodgers, C. D. (2000), *Inverse Methods for Atmospheric Sounding: Theory and Practice*, 238 pp., World Scientific, Singapore.
- Rose, T., S. Crewell, U. Löhnert, and C. Simmer (2005), A network suitable microwave radiometer for operational monitoring of the cloudy atmosphere, *Atmos. Res.*, *75*(3), 183–200.
- Rosenkranz, P. (1998), Water vapor microwave continuum absorption: A comparison of measurements and models, *Radio Sci.*, *33*(4), 919–928.
- Saunders, R. W., M. Matricardi, and P. Brunel (1999), An improved fast radiative transfer model for assimilation of satellite radiance observations, *Q. J. R. Meteorol. Soc.*, *125*(556), 1407–1425.
- Saunders, R. W., M. Matricardi, and A. Geer, (2009), RTTOV9.1 User Guide, *Tech. Rep.*, *NWPSAF-MO-UD-016*, EUMETSAT, Eumetsat Allee 1D-64295, Darmstadt, Germany, [Available at <http://research.metoffice....rttov9.html>].
- Schmetz, J., P. Pili, S. Tjemkes, D. Just, J. Kerkmann, S. Rota, and A. Ratier (2002), An introduction to Meteosat Second Generation (MSG), *Bull. Am. Meteorol. Soc.*, *83*, 977–994.
- Shephard, M. W., S. A. Clough, V. H. Payne, W. L. Smith, S. Kireev, and K. E. Cady-Pereira (2009), Performance of the line-by-line radiative transfer model (LBLRTM) for temperature and species retrievals: IASI case studies from JAIVEx, *Atmos. Chem. Phys.*, *9*, 7397–7417.
- Smith, W. L., W. F. Feltz, R. O. Knuteson, H. E. Revercomb, H. M. Woolf, and H. B. Howell (1999), The retrieval of planetary boundary layer structure using ground-based infrared spectral radiance measurements, *J. Atmos. Oceanic Technol.*, *16*, 323–333.
- Soden, B., et al. (2000), An intercomparison of radiation codes for retrieving upper-tropospheric humidity in the 6.3-mm band: A report from the first GvAP workshop, *Bull. Am. Meteorol. Soc.*, *81*, 797–808.
- Turner, D. D., D. C. Tobin, S. A. Clough, R. G. Ellingson, E. J. Mlawer, R. O. Knuteson, H. E. Revercomb, T. R. Shippert, and W. L. Smith (2004), The QME AERI LBLRTM: A closure experiment for downwelling high spectral resolution infrared radiance, *J. Atmos. Sci.*, *61*, 2657–2675, doi:10.1175/JAS3300.1.
- Turner, D. D., M. P. Cadetdu, U. Löhnert, S. Crewell, and A. M. Vogelmann (2009), Modifications to the water vapor continuum in the microwave suggested by ground-based 150-GHz observations, *IEEE Trans. Geosci. Remote Sens.*, *47*(10), 3326–3337.
- Westwater, E. R. (1997), Remote sensing of tropospheric temperature and water vapor by integrated observing systems, *Bull. Am. Meteorol. Soc.*, *78*, 1991–2006.